ISSN 0023-1584, Kinetics and Catalysis, 2015, Vol. 56, No. 1, pp. 31–42. © Pleiades Publishing, Ltd., 2015.

Effect of the *n*-Butanol Addition on Cyclopentadienyl Radical Formation during Benzene Combustion[1]

N. Boussid[a, b] and Y. Rezgui[c, *]

[a] *Faculté des Sciences et de la Technologie, Département des Sciences et de la Technologie, Filière Génie des procédés, Université d'El Oued, Algérie*

[b] *Département de Génie des procédés, Université de Ouargla, Algérie*

[c] *Laboratoire de Chimie Appliquée et Technologie des Matériaux, Université d'Oum El Bouaghi, Algérie*

**e-mail: yacinereference@yahoo.com*

Received April 22, 2014

Abstract—The PREMIX code in conjunction with Chemkin II and models resulting from the merging of validated kinetic schemes describing the oxidation of the components of the *n*-butanol–benzene mixtures were used to investigate the effect of *n*-butanol addition on the formation–depletion of cyclopehtadienyl radical (C_5H_5), a soot precursor in the flames of mixtures of *n*-butanol–benzene formed under fuel-rich conditions. The first part of this study deals with the validation of the proposed combined model on benzene and *n*-butanol flames. The second part describes the dependence of the amount of cyclopentadienyl radical on the percentage of benzene replacement by oxygenate additive. The third part deals with the causes of the variation of mole fractions of this species with *n*-butanol. The principal objective of this work was to obtain fundamental understanding of the mechanisms through which an oxygenate affects amounts of C_5H_5. It was found that the cyclopentadienyl radical concentration was lower in the flame of the *n*-butanol–benzene fuel mixture than in the pure benzene flame.

DOI: 10.1134/S0023158415010048

In response to the depletion of fossil fuels and to the global environmental concerns, researchers focused their interest on the development of cleaner and sustainable energy sources [1–6]. It was found that renewable biofuels, such as bioalcohols, are promising candidates for use as transportation fuels [7–13]. Ethanol is a first generation biofuel that is used as a pure fuel or as a fuel blend for transport vehicles, today, it accounts for over 90% of the total biofuel production worldwide [14, 15]. Ethanol as a biofuel has many advantages. Ethanol fuelled vehicles reduce dependence on fossil fuels and produce lower levels of exhaust emissions such as nitrogen oxides (NO_x), unburned hydrocarbons, soot and carbon monoxide [16–19]. Nevertheless, using ethanol as a fuel suffers from a number of drawbacks, including low energy density, low viscosity, low lubricity, high vapour pressure and high solubility in water which negatively impact vehicle fuel economy and prevent ethanol transportation via pipelines like pure gasoline [20–22]. For these reasons, recent research focus was shifted to higher alcohols [23–26].

Compared to ethanol, *n*-butanol is a new promising bio-fuel with higher energy content, higher viscosity, higher flash point, lower vapor pressure and lower solubility in water, making it preferable to ethanol for blending with fossil fuels. In addition, *n*-butanol can be produced by advanced fermentation techniques using various feed stocks [27]. For these reasons *n*-butanol received an increased attention in the recent combustion research. In terms of fundamental combustion, neat butyl alcohols have been studied in flames [28–37], jet stirred reactors [35, 38–42], flow reactors [43–45] and shock-tubes [46–53]. The results of these studies led to the development of comprehensive kinetic butanol combustion models [30, 31, 35, 41, 44, 48, 49, 53–56]. On the other hand, several recent investigations into the use of neat biobutanol and biobutanol blended with classic fuels in spark ignition engines [57–61], direct injection and HCCI engines [62–69] showed that the C_4 alcohols are very challenging alcohols competitor for the use as a fuel in these engines [23].

Although the decomposition pathways of butanol and its isomers were widely studied, insufficient attention was paid to the process of formation of soot precursors and polycyclic aromatic hydrocarbons (**PAHs**) [70]. To the best of our knowledge, there was no study on the effect of butyl alcohols on the formation of cyclopentadienyl radical, which is considered as one of the main soot precursors [71–73].

The aim of this paper is to present potential benefits of using renewable fuel blends, in this case *n*-butanol, in terms of cyclopentadienyl radical reduction. This investigation is mainly focused on the modeling rela-

[1] The article is published in the original.

tion between the C_5H_5 amounts and fuel composition as well as on the formation-consumption pathways of this species. However, the objective of this modeling study was the analysis of the reaction pathways involved in the formation–depletion of cyclopentadienyl radical rather than a theoretical reproduction of the experimental data.

SELECTED COMPOUNDS

The reduction of the polycyclic aromatic hydrocarbons (PAHs) and soot formation in flames is a primary focus of current combustion researches because of the potency of some of the PAH isomers in inducing mutations and cancer [71, 74–76]. These heavy and stable compounds, particularly benzo[a]pyrene, are metabolized by human body to high electrophilic chemical species (epoxies), which tend to disturb cellular division through their addition on proteins and DNA [77, 78].

PAH growth models generally agree that the formation of PAHs starts from an aromatic species, a benzene molecule or a phenyl radical [79]. It is generally believed that, under fuel-rich conditions, the PAHs are formed by sequential activation of neighboring aromatic sites by hydrogen atom abstraction, followed by multiple additions of the aryl radical to acetylene molecules, and cyclization to the next higher order ring (HACA mechanism) [80, 81]. However, this model falls short in predicting many of the experimental observations [82] and it appeared that new reaction mechanisms for PAH formation must be invoked. Melius et al. proposed that in aliphatic hydrocarbon flames, the larger aromatics originate from resonance-stabilized cyclopentadienyl radicals (C_5H_5) and postulated a radical-radical mechanism that describes the naphthalene formation from two C_5H_5 radicals [71]. Mullholland et al. studied the PAH formation and growth and confirmed that higher aromatic compounds could be formed via a radical-molecule mechanism in which cyclopentadienyl radical plays a crucial role [83]. The importance of this latter pathway and the cyclopentadienyl moities in the growth of the PAH compounds was also reported by Violi et al. [84, 85]. All the proposed mechanisms assume that the formation of the first aromatic ring was the rate-limiting step in the formation of polyaromatic hydrocarbons and soot. Accordingly, much attention was given to this process [86, 87].

Due to the pertinent role of C_6H_6 and C_5H_5 in forming aromatics and PAHs, these species were selected in the present work.

Finally, Detilleux and Vandooren suggested the analysis of one-dimensional laminar premixed low-pressure benzene flame structures as an attractive way to investigate PAH formation pathways, in which the first aromatic ring does not need to be formed. Thus, avoiding the uncertainties associated with the formation of the first ring [77] and taking this suggestion into account, the C_6H_6 was chosen as a reactant model.

MODELING APPROACH

All the simulations have been performed using the PREMIX code for modeling premixed laminar stabilized flames [88]. The program input includes forward reaction rates and thermodynamic polynomials for all of the participating species in addition to temperature profile, pressure, mass flow rate through the burner and concentrations of the reactants.

The global gas phase chemical kinetic mechanism, used to describe pyrolysis and oxidation of the benzene-butanol mixtures, was built up based on the recent kinetics literature for benzene, butanol, and a baseline of small hydrocarbon species. The mechanism of Richter and Howard (**Rich**), elaborated especially for the description of the benzene combustion and oxidation [89], was taken as the base mechanism. To model the *n*-butanol combustion, additional reactions were added to the core mechanism from the model of Sarathy et al. (**Sar**), proposed especially for the description of the butyl alcohols combustion and oxidation [56]. Hydrogen abstraction and monomolecular decomposition, as well as reactions of the resulting products that eventually produced species present in the benzene mechanism were the selected reactions from the alcohol kinetic scheme.

The model of Richter and Howard was assessed against experimental data issued from studies conducted in four one-dimensional laminar premixed low-pressure ethylene, acetylene, and benzene flames at equivalence ratios (Φ) of 0.75 and 1.9 (C_2H_4) [90, 91], 2.4 (C_2H_2) [92], and 1.8 (C_6H_6) [93, 94]. As indicated by the authors, the mechanism successfully reproduces the formation of the main combustion products, and the formation and depletion of major intermediates including radicals. Richter's model includes reactions subsets of species up to $C_{16}H_{10}$ and consists of 157 chemical species and 872 reactions. This reaction mechanism is provided for low-pressure and atmospheric pressure conditions and takes into account the pressure dependence of chemically activated reactions.

The model of Sarathy et al., developed for the combustion and oxidation of the four butanol isomers, included comprehensive low and high temperature pathways with reaction rate constants derived using rate rules. The experimental validation targets for this model included low pressure premixed flat flames [32, 34], atmospheric pressure premixed laminar flame velocities [36, 50], elevated pressure rapid compression machine [95] and shock tube ignition delay [49, 53], as well as jet-stirred reactor species profiles [41, 42]. As indicated by the authors, the agreement with these various data sets, spanning a wide range of temperatures and pressures, was reasonably good. This

mechanism was composed of 418 species evolved in 2336 reactions.

The thermochemical dataset and the transport dataset used for modeling the global mechanism were originally taken from the base chemical kinetic models and that within the combined mechanism, all reactions and values of the rate coefficients were kept unchanged as compared to those in the base mechanisms. The combined mechanism is composed of 521 species evolved in 3020 reactions.

To explore the fundamental kinetic causes for the fuel composition effects, a systematic approach was taken such that the effect of temperature is isolated from the fuel composition effect. The temperature profiles of all of the flames were kept nearly constant by adjusting the total cold gas velocity. This task was accomplished by means of the PREMIX code with solving the energy equation.

Vandooren et al. reported the experimental study of the behavior of the neat benzene flame (Table) [96, 97]. The blended fuels were formed by incrementally adding 4 wt % of *n*-butanol to the neat benzene flame and by keeping the inert mole fraction (argon) and the equivalence ratio constants.

RESULTS AND DISCUSSION

Model Validation

To verify that the added reactions, in the combined model, did not change in any substantial way the base mechanisms, the results of benzene and *n*-butanol combustion were compared with data evolved from the augmented and the base mechanisms.

Benzene combustion. In order to assess the prediction power of the global mechanism elaborated for (100% benzene + 0% *n*-butanol) flame conditions, experimental data from Vandooren et al. [96, 97] and from Bittner and Howard [94] were compared with corresponding model predictions. In the first case [96, 97], the flame structure of a sooting one-dimensional premixed benzene–oxygen–argon flame burning at 45 mbar with a fuel equivalence ratio (Φ) of 2.0 was measured using gas chromatography. Fifteen chemical species were detected, including permanent gases of combustion (O_2, CO_2, H_2O, CO, and H_2) and ten hydrocarbons (from C_1 to C_6). Errors on experimental profiles of 10 and 20% should be considered for chemical species that are directly calibrated and for unstable compounds, respectively. The temperature profile was measured by using Pt/Pt–10% Rh thermocouple, 0.1 mm in diameter, coated with a thin layer of Y_2O_3–BeO ceramics. Radiation losses were corrected by electrical compensation. In the second case [94], the structure of a near-sooting flat low-pressure laminar benzene-oxygen-argon flame was studied using a molecular beam mass spectrometer system. The flame was investigated at a pressure of 2.67 kPa, a cold gas velocity of 0.5 m/s and a temperature of 298 K. The weight percentages of reactants were 13.5 (C_6H_6), 56.5 (O_2) and 30.0 (Ar) and the fuel equivalence ratio was 1.8. Temperatures were measured using butt-welded thermocouples made from 0.076 mm diameter Pt/Pt–13% Rh wires. A BeO–Y_2O_3 coating was used to minimize catalytic effects and an electrical heating technique was used to compensate for radiation losses. Measurement uncertainty in the flame unperturbed by probe effects is estimated to be +50 K.

Models predictions (combined and Richter model) and experimental data for benzene, oxygen, acetylene, and cyclopentadiene in the benzene flame investigated by Vandooren et al. [97] are compared in Fig. 1a. It can be seen that both combined and Richter model overestimate benzene mole fraction, whereas predictions of oxygen concentrations agree well with the experimental points up to a distance of about 0.6 cm from the burner surface. At the same time, the predicted oxygen consumption for the points lying farther from the burner is slightly slower than for those in the experi-

Parameters of *n*-butanol-benzene flames

Flame	Equivalence ratio (Φ)	G, 10^{-3} g cm^{-2} s^{-1}	Composition, mole fractions			
			C_6H_6	NC_4H_9OH	O_2	Ar
Neat flame [97]	2	3.102	0.1200	0	0.44	0.44
Flame with 4% *n*-butanol	2	3.192	0.0981	0.0234	0.4384	0.44
Flame with 8% *n*-butanol	2	3.435	0.0775	0.0480	0.4345	0.44
Flame with 12% *n*-butanol	2	3.526	0.0560	0.0736	0.4305	0.44
Flame with 16% *n*-butanol	2	3.638	0.0334	0.1003	0.4263	0.44
Flame with 20% *n*-butanol	2	3.961	0.0099	0.1283	0.4218	0.44

mental profiles. On the other hand, the two considered models underestimate acetylene mole fractions, whereas the cyclopentadiene concentrations are well predicted.

In the case of the nearly sooting benzene flame [94] (Fig. 1b), the computed benzene, acetylene, propargyl and cyclopentadienyl radicals mole fractions agree well with the experimental values, whereas concentrations of oxygen are overestimated especially those positioned on the distance above 0.9 cm from the surface burner.

In the two studied cases, both models (the combined and Richter) behave similarly, thus, it could be concluded that only minor differences were observed between the combined model and the model of Richter.

***n*-Butanol combustion.** In order to verify that the added reactions, in the combined model, did not change in any substantial way the base mechanism (mechanism of Sarathy), results of *n*-butanol combustion were compared with the data consistent with the augmented mechanism and the mechanism of Sarathy. The used experimental sets were those of Osswald et al. [32] and Hansen et al. [34]. In the first case [32], the flame structure of a one-dimensional premixed *n*-butanol–oxygen–argon flame burning at 40 mbar with a fuel equivalence ratio (Φ) of 1.7 was measured by two different molecular beam mass spectrometers, using the combined capabilities of a high energy-resolution photoionization (PI) system located at the National Synchrotron Radiation Laboratory (NSRL) in Hefei (China) together with a high mass-resolution electron ionization (EI) instrument located in Bielefeld (Germany). As indicated by Sarathy et al. [56], this powerful combination of molecular beam sampling techniques allows to conduct the identification and quantification of stable and radical species based on either their elemental composition (EI) or their ionization threshold (PI). The latter approach serves to determine the respective isomeric composition in many cases. In total, 57 chemical compounds, including radical and isomeric species, were unambiguously assigned and detected quantitatively in the *n*-butanol flame.

In the second case [34], the combustion chemistry of *n*-butanol was studied in flat, premixed, laminar low-pressure flame (42.8% O_2, 50.0% Ar, $\Phi = 1.0$, $P =$ 15 Torr and $v = 96.1$ cm/s). The flame was stabilized at a low pressure on a water-cooled 6 cm diameter stainless steel McKenna burner and the temperature profile was measured with laser-induced fluorescence (LIF). The accuracy of the temperature measurements was estimated to be ±150 K in the postflame and reaction zones and is somewhat larger in the preheat zone, where the OH concentration is much smaller and its concentration gradient is much sharper.

Predicted and experimental data are compared in Figs. 2a and 2b. Results for the fuel rich conditions (Osswald flame: Fig. 2a) indicate that predicted acetylene mole fractions (**C_2H_2**) are half of experimental values. However due to the experimental uncertainties, predictions within a factor of 2–3 of the experimental data are considered good [56]. Besides, the obtained results indicate that both models predict that ethenol is formed in higher yields than acetaldehyde, while the experimental data show the reverse trend. As reported by Sarathy et al. [56], the predicted ethenol formation occurred through H-atom abstraction from the alpha-carbon followed by beta-scission to form C_2H_5 and ethenol, whereas the main acetaldehyde (**Acetal**) formation is the ethenol H catalysed enol-keto isomerization reaction. Thus, a rise in the rate of these reactions would improve the models predictions of acetaldehyde. In addition, the two models accurately predict the mole fraction of formaldehyde and ketene (**Form**). This perfect matching can be ascribed to the fact that formaldehyde can be formed directly from *n*-butanol following abstraction from the hydroxyl moiety and subsequent beta-scission of the C_4H_9O radical. This fuel-direct pathway rationalizes the higher predicted and measured concentrations [56].

Results for the stoichiometric conditions (Hansen flame: Fig. 2b) indicate that the reactivity of *n*-C_4H_9OH and O_2 are well predicted by the two models, whereas the predicted reactivities of C_2H_2 and CH_2O are higher than the measured values. On the other hand, a good agreement is found between calculations and measurements in the case of C_3H_3, whereas a fair disagreement is found between the values suggested by the models and the measured values for CH_3O.

The calculations show that the two studied models (the combined one and the one of Sarathy) behave similarly in all conditions and that only minor differences are observed between the combined model and the model of Sarathy. Thus, it can be stated that the added reactions, in the combined model, introduce no appreciable change the base mechanism (mechanism of Sarathy).

C_5H_5 Mole Fractions

This section describes the yield behavior of cyclopentadienyl radical as a function of the fraction of *n*-butanol in the fuel mixture.

The dependence of cyclopentadienyl radical mole fractions (**C_5H_5**) on the fraction of *n*-butanol in the mixture fuel is depicted in Fig. 3a. It can be seen that the same trends were observed for any level of the benzene replacement by oxygenate additive. In all cases, the C_5H_5 concentration increases with distance above the burner, reaches a maximum at about 0.9 cm from the burner surface, and decreases thereafter. Besides, C_5H_5 levels showed a dramatic change in peak height with doping, they decreased monotonically and linearly with increasing the percentage of the *n*-butanol in the mixture. Cyclopentadienyl radical amounts were the highest in the 0% *n*-butanol flame (3.62 ×

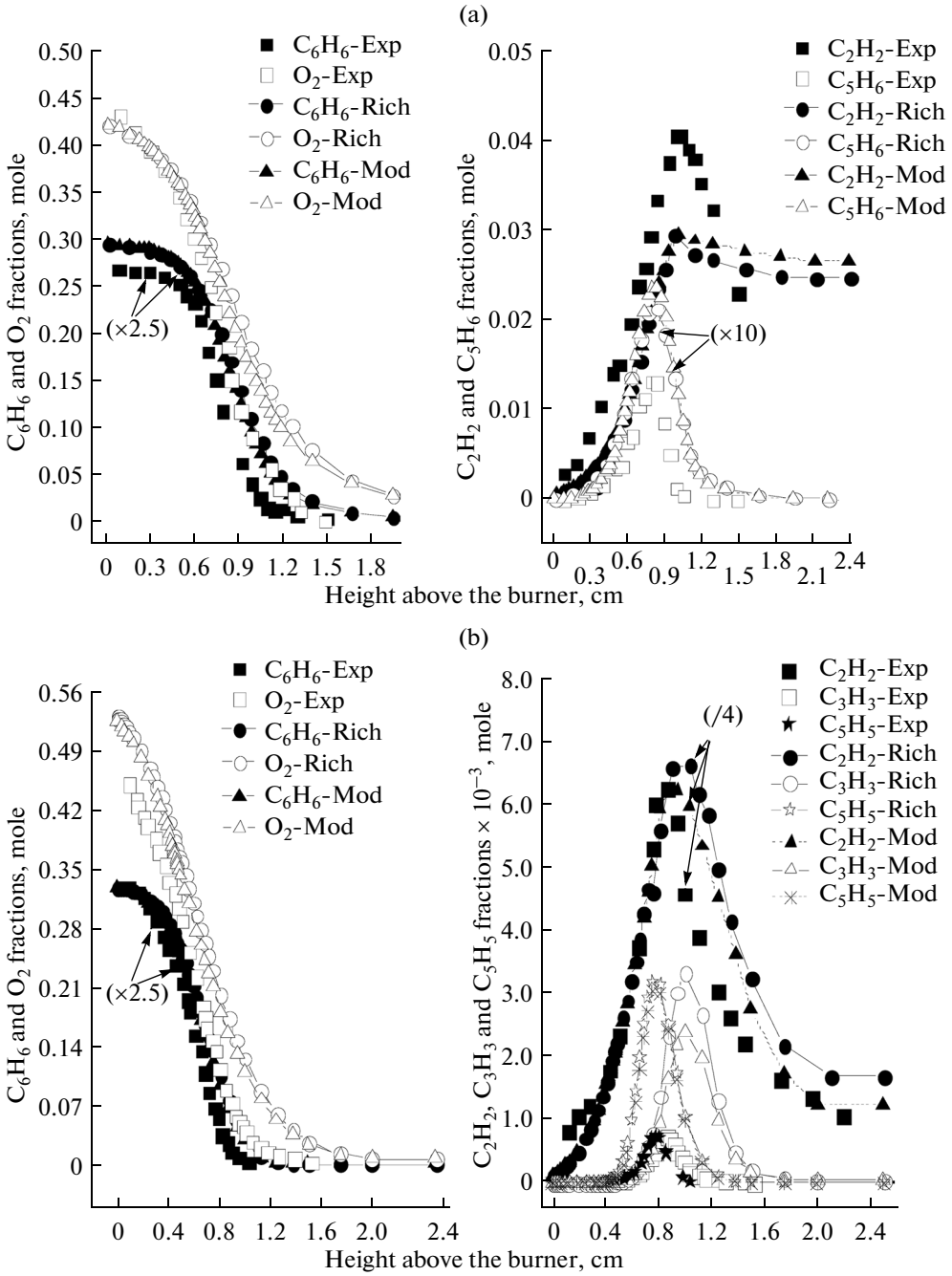

Fig. 1. Experimental (symbols) and modelled (symbols + lines) mole fraction profiles for the major species in benzene flames (Vandooren flame) (a) and (Bittner and Howard flame) (b) as a function of distance from the burner.

10^{-3} moles) and the lowest in the 20% *n*-butanol flame (2.18×10^{-4} moles), which means a 93% decrease.

These findings might lead to wrong conclusions on the real efficiency of *n*-butanol in decreasing C_5H_5 amounts, because we cannot assess this effect except when eliminating the effect of the benzene reduction induced by the *n*-butanol replacement. The data depicted in Fig. 3b show clearly that, whatever the *n*-butanol amount in the fuel mixture, a decrease in C_5H_5 was higher than that observed for C_6H_6. Besides, the slope of the difference (**C_5H_5–C_6H_6**) was not constant and displayed an increasing trend until the yield of *n*-butanol reaches a 16% level. These observations rule out the theory that a decrease in C_5H_5 was due to the combination of the beneficial effect of decreasing yields of *n*-butanol and C_6H_6 and that 16% *n*-butanol exhibited the most noticeable effect on the loss of C_5H_5.

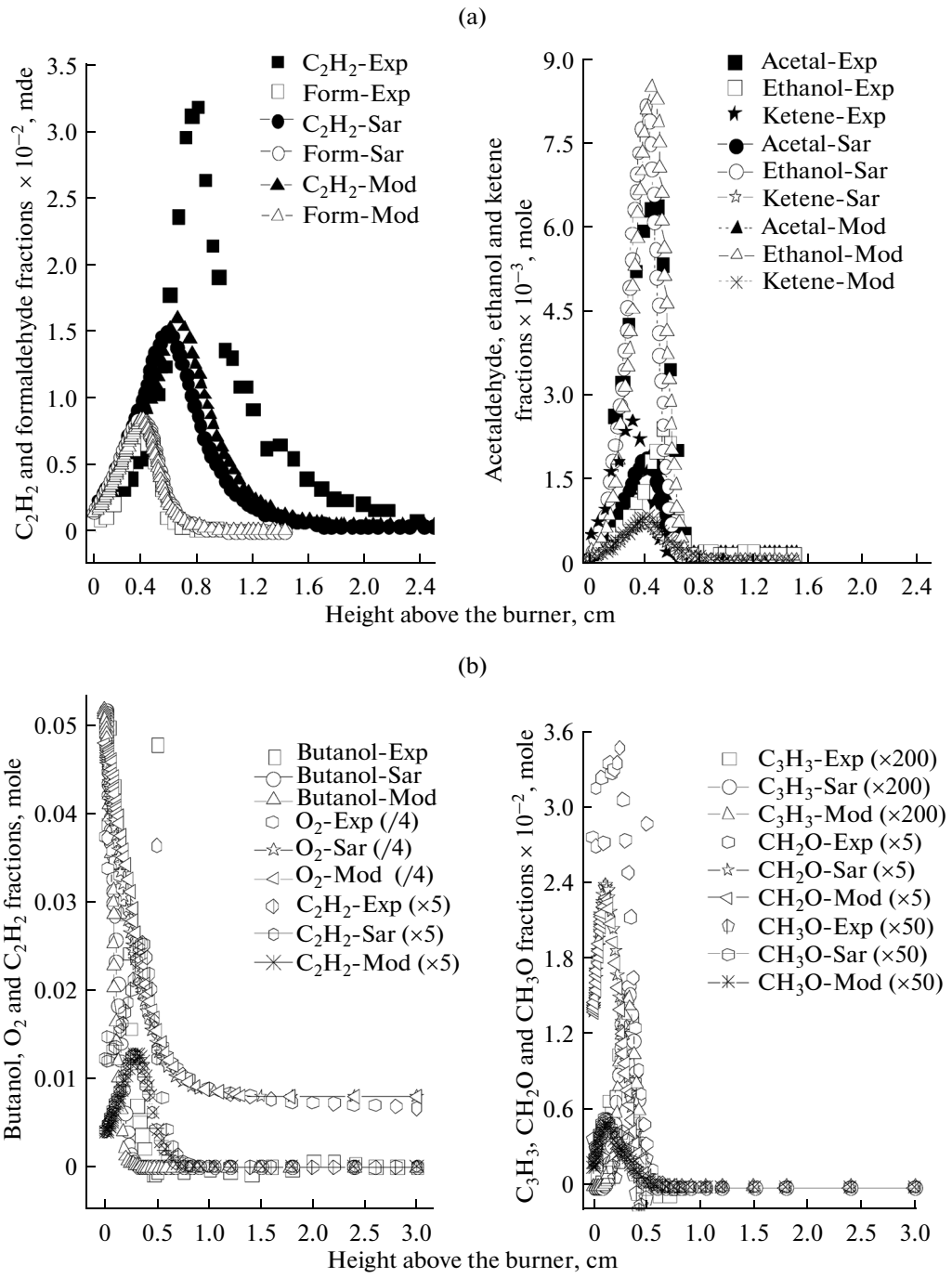

Fig. 2. Experimental (symbols) and modelled (symbols + lines) mole fraction profiles for the major species in *n*-butanol flames (Osswald flame) (a) and (Hansen flame) (b) as a function of distance from the burner.

Noteworthy, that, whatever the alcohol content (%) in the fuel mixture, the effectiveness of *n*-butanol in reducing C_5H_5 amounts is high compared to that of ethanol at the same concentration level (see Fig. 4). The difference in effectiveness increases linearly with increasing the alcohol percentage in the fuel mixture implying that *n*-butanol was more efficient in reducing C_5H_5 at high loadings.

Pathway Analysis

In this section, the main reaction pathways of the neat benzene fuel as well as of the flame doped with 20% *n*-butanol was tracked by performing a reaction flux analysis. In this respect, rates of consumption and production were computed for the selected species (C_5H_5) that is suspected as a soot precursor. In addition, an analysis was conducted to identify any differ-

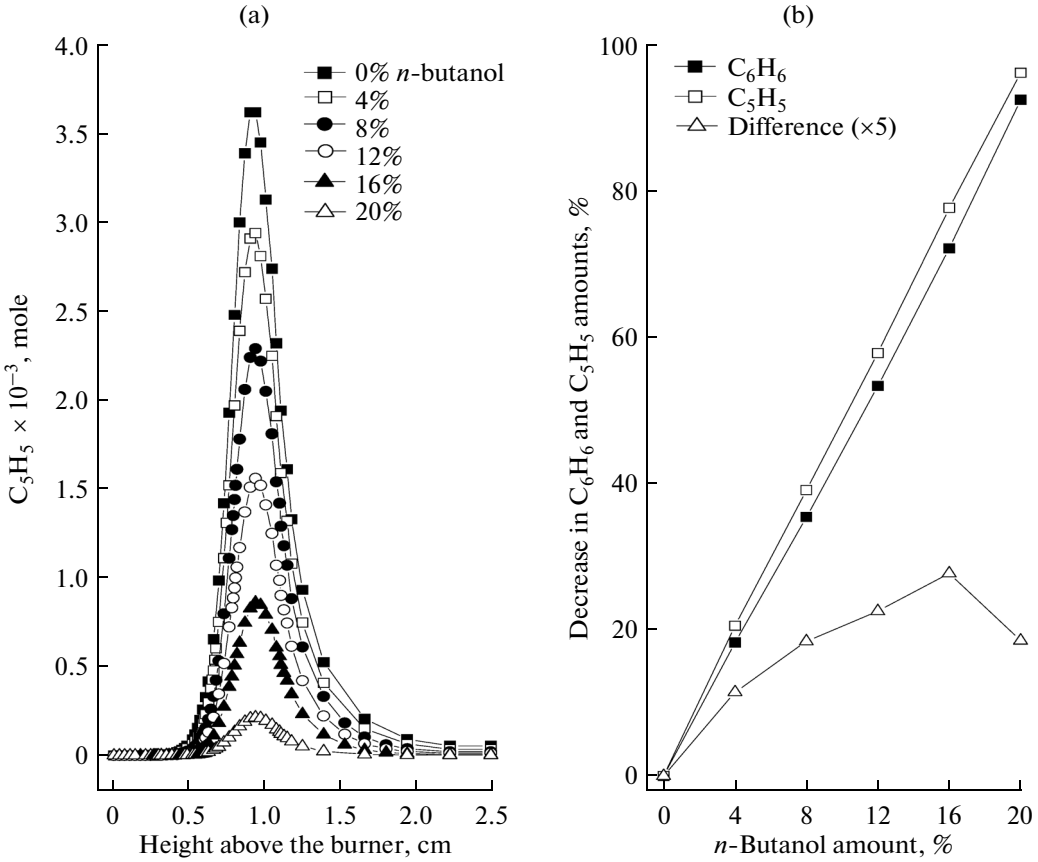

Fig. 3. Effect of *n*-butanol on the mole fraction of cyclopentadienyl radical (a) and on the decreasing amounts of C_6H_6 and C_5H_5 (b).

ences observed between the blended fuels and the neat benzene flame. This analysis was performed using the appropriate subroutines in the Chemkin package (CKQYP, CKCONT) that systematically computes the rate of production–consumption of each species [88].

In this section, only the main reactions, which have an important role in chemicals belonging to the studied system, will be taken into account. The numbers in parentheses correspond to the numbers of reaction in the combined *n*-butanol-benzene mechanism.

C_5H_5 formation-depletion routes. Flux analysis showed that, regardless of the benzene replacement percentage by oxygenate additive, the monomolecular decomposition of the phenoxy radical (670) as well as hydrogen abstraction from the cyclopentadiene (C_5H_6), with H and CH_3 (reactions 592 and 601, respectively) were the most important routes in the formation of the cyclopentadienyl radical (C_5H_5):

$$C_5H_6 + H = C_5H_5 + H_2, \quad (592)$$

$$C_5H_6 + CH_3 = C_5H_5 + CH_4, \quad (601)$$

$$C_6H_5O = C_5H_5 + CO. \quad (670)$$

The monomolecular decomposition was the predominant channel with a 80.9% contribution in the case of the neat benzene flame and with a 63.9% contribution in the case of the flame doped with 20% of *n*-butanol. Whereas the hydrogen abstraction with CH_3 was the minor channel contributing with 0.9 and 8.3% in the case of the flames containing 0 and 20% *n*-butanol, respectively. Besides, it was found that

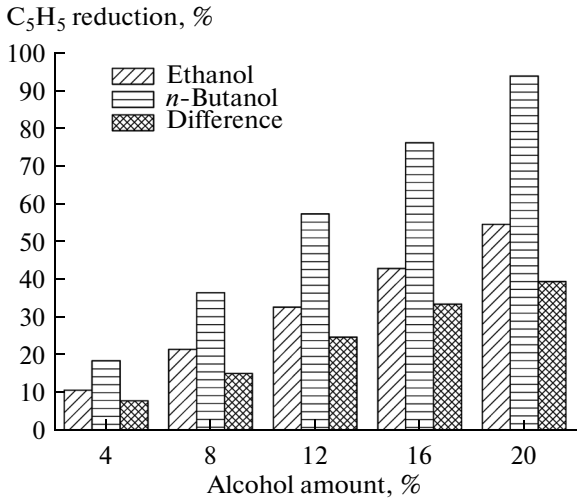

Fig. 4. Comparison between the ability of the two alcohols, ethanol and *n*-butanol, in reducing C_5H_5 amounts.

reaction rates 670 and 592 decreased continuously with a rise in the *n*-butanol amount, whereas the rate of the reaction 601 increased to reach a maximum at 8% yield of butanol and then decreased (Fig. 5).

On the other hand, the cyclopentadienyl radical depletion analysis demonstrated that reactions of C_5H_5 with H, O, OH and C_3H_6 (reactions 575, 564, 583, 580, 565 and Rev 609, respectively), as well as the C_5H_5 decomposition leading to C_3H_3 and C_2H_2 (reaction 576) and the C_5H_5 bimolecular combination leading to $C_{10}H_8$ (reaction 773) were the most important:

$$C_5H_5 + H = C_5H_4 + H_2, \quad (564)$$

$$C_5H_5 + OH = C_5H_4 + H_2O, \quad (565)$$

$$C_5H_5 + H = C_5H_6, \quad (575)$$

$$C_5H_5 = C_3H_3 + C_2H_2, \quad (576)$$

$$C_5H_5 + O = CH_2CHCHCH + CO, \quad (580)$$

$$C_5H_5 + O = C_5H_4O + H, \quad (583)$$

$$C_5H_6 + C_3H_5 = C_5H_5 + C_3H_6, \quad (\text{Rev } 609)$$

$$2\,C_5H_5 = C_{10}H_8 + 2\,H. \quad (773)$$

The modeling results revealed that, whatever the *n*-butanol percentage in the fuel mixture, the reaction 575 was the major route, contributing with 36.1 and 43.2%, and the reaction 609 was a minor route with a contribution of 0.9 and 9.9% in the case of flames with 0 and 20% *n*-butanol, respectively. Besides, all the rates of the C_5H_5 consumption reaction exhibited a decreasing trend with a rise in the *n*-butanol percentage in the fuel (Fig. 5). These results led to the conclusion that *n*-butanol addition induced a decrease in the rates of the reactions of cyclopentadienyl radical formation as well as in the rates of its consumption.

A detailed inspection of the pathway analysis showed that the cyclopentadienyl radical formation followed the sequence depicted in Scheme.

Main routes in the transformation of benzene to cyclopentadienyl radical mixture

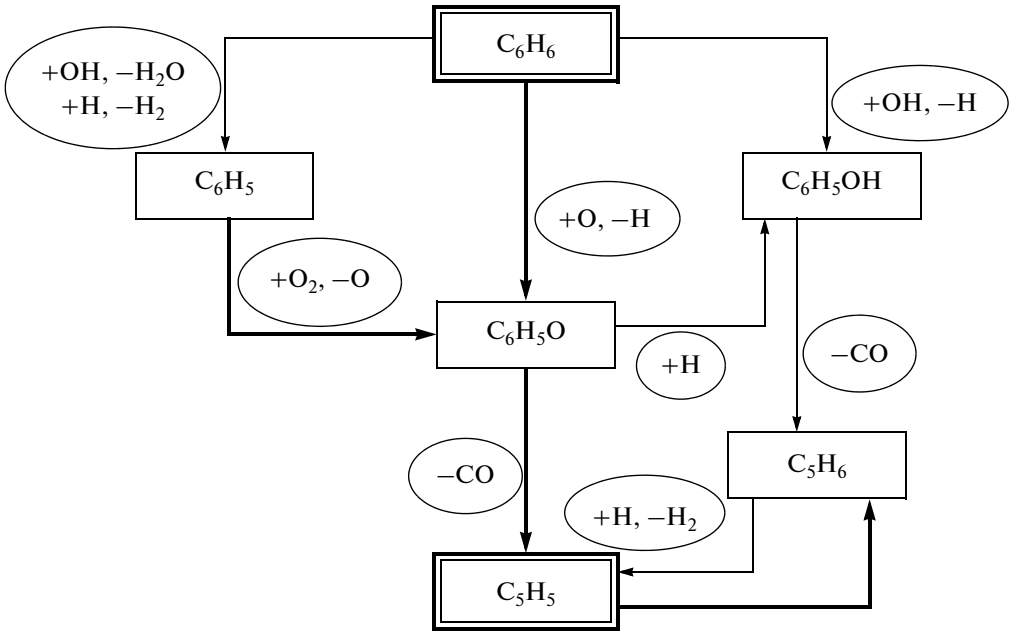

Sheme.

The Scheme implies that regardless of the *n*-butanol amount, C_6H_6 and C_6H_5 were the principal source of the cyclopentadienyl radical. It is obvious that amounts of benzene formed were automatically reduced on adding *n*-butanol. It can be thus inferred that yields of C_5H_5 were related to the concentrations of the phenyl radical in the mixture. On the other hand, analysis of the phenyl radical formation flux showed that hydrogen abstraction from benzene was the dominant pathway:

$$C_6H_6 + H = C_6H_5 + H_2, \quad (646)$$

$$C_6H_6 + OH = C_6H_5 + H_2O. \quad (649)$$

Accordingly, the yield of C_6H_5 can be related to $[C_6H_6] \cdot \{([OH]/[H_2O]) + ([H]/[H_2])\}$, noted as **R1**. Figure 5 portrays the variation of this ratio with *n*-butanol content. It can be seen that the ratio decreases with increasing amounts of n-C_4H_9OH in the fuel mixture. It decreases from 9.3×10^{-4} in the case of the neat benzene flame to 5.2×10^{-5}, in the case of the flame with 20% *n*-butanol, indicating a 17.8 fold reduction. This decrease led to a decrease in the C_6H_5 mole fraction and consequently to a lowering in the C_5H_5 concentration.

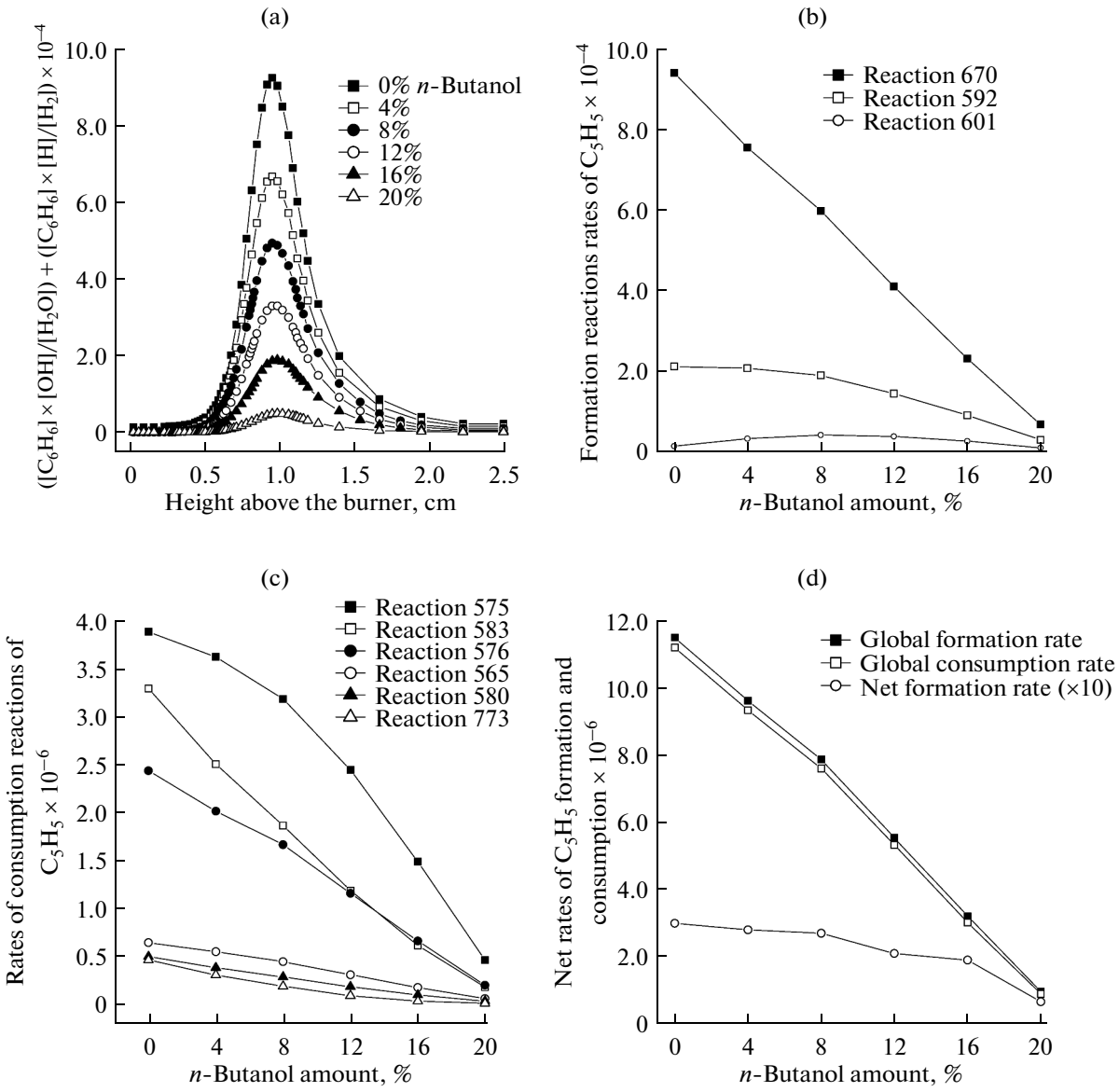

Fig. 5. Effect of *n*-butanol on cyclopentadienyl radical formation (a) and consumption reactions (b)–(d).

Figure 6 compares the cyclopentadienyl radical amounts observed for ethanol–benzene and *n*-butanol–benzene flames. It can be seen that whatever the benzene replacement percentage by the oxygenate additive, the C_5H_5 mole fraction in the case of *n*-butanol was lower than in the case of ethanol. The difference was more pronounced at higher alcohol levels. Besides, the pathway analysis results revealed that, in the two cases (ethanol and *n*-butanol), the same reactions were evolved in the cyclopentadienyl radical formation-depletion routes implying that the phenyl radical amounts governed the C_5H_5 concentrations in both cases. However, as indicated above, the C_6H_5 amount was directly related to the value of $[C_6H_6] \cdot \{([OH]/[H_2O]) + ([H]/[H_2])\}$. From the results of Fig. 6, it is obvious that the higher is the alcohol concentration in the fuel mixture, the lower is the value of R1 and the lower is the C_5H_5 mole fraction. A decrease in R1 induced by the alcohol doping was more pronounced in the case of *n*-butanol as compared to ethanol implying that the butyl alcohol was more efficient than ethanol in reducing C_5H_5 amounts especially at higher concentrations.

Thus, this modeling study gives evidence that:

1—mole fraction of the studied soot precursor (C_5H_5) showed a dramatic change in peak height with doping. It decreased monotonically and linearly with increasing percentage of the *n*-butanol in the mixture. This decrease was the highest for the 20% *n*-butanol flame;

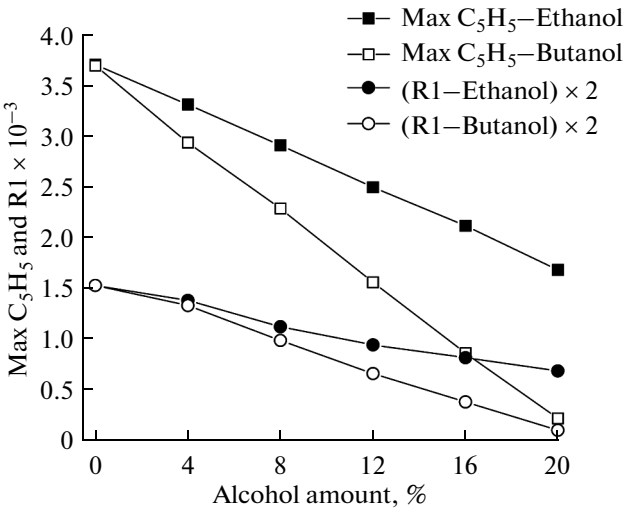

Fig. 6. Effect of the alcohol amount (ethanol and *n*-butanol) on maximum content C_5H_5 (max C_5H_5) and R1.

2—the decrease in the concentration of cyclopentadienyl radical was due to the combined effect of *n*-butanol addition and benzene replacement by the oxygenated additive;

3—regardless the *n*-butanol amount in the fuel mixture, the cyclopentadienyl radical (C_5H_5) formation was governed by the monomolecular decomposition of the phenoxy radical as well as the hydrogen abstraction from the cyclopentadiene (C_5H_6), with H and CH_3, whereas reactions of C_5H_5 with H, O, OH and C_3H_6 as well as the C_5H_5 decomposition leading to C_3H_3 and C_2H_2 and the C_5H_5 bimolecular combination leading to $C_{10}H_8$ were the most important reactions in the cyclopentadienyl radical depletion. Besides, both formation and consumption rates of the cyclopentadienyl radical exhibited a decreasing trend with increasing concentration of *n*-butanol.

REFERENCES

1. Kuang, C.L., Jason, Y.W.L., and Violi, A., *Fuel*, 2012, vol. 92, p. 16.
2. Pidol, L., Lecointe, B., Starck, L., and Jeuland, N., *Fuel*, 2012, vol. 93, p. 329.
3. Karavalakis, G., Durbin, T.D., Shrivastava, M., Zheng, Z., and Villela, M., *Fuel*, 2012, vol. 93, p. 549.
4. Chen, L., Stone, R., and Richardson, D., *Fuel*, 2012, vol. 96, p. 120.
5. Maricq, M.M., *Combust. Flame*, 2012, vol. 159, p. 170.
6. Gaffney, J.S., Marley, N.A., and Blake, D.R., *Atmos. Environ.*, 2012, vol. 56, p. 161.
7. Anderson, J.E., Dicicco, D.M., Ginder, J.M., Leone, T.G., Raney-Pablo, H.E., and Wallington, T.J., *Fuel*, 2012, vol. 97, p. 585.
8. Gerasimov, I.E., Knyazkov, D.A., Yakimov, S.A., Bolshova, T.A., Shmakov, A.G., and Korobeinichev, O.P., *Combust. Flame*, 2012, vol. 159, p. 1840.
9. Yoon, S.H. and Lee, C.S., *Fuel*, 2012, vol. 97, p. 887.
10. Winther, M., Moller, F., and Jensen, T.C., *Atmos. Environ.*, 2012, vol. 55, p. 144.
11. Song, J., Yao, C., Liu, S., and Xu, H., *Energy Fuels*, 2008, vol. 22, p. 3806.
12. Wang, J., Struckmeier, U., Yang, B., Cool, T.A., Osswald, P., Kohse-Hoinghaus, K., Kasper, T., Hansen, N., and Westmoreland, P.R., *J. Phys. Chem. A*, 2008, vol. 112, p. 9255.
13. Westbrook, C.K., Pitz, W.J., and Curran, H.J., *J. Phys. Chem. A*, 2006, vol. 110, p. 6912.
14. Kohse-Hoinghaus, K., Osswald, P., Cool, T.A., Kasper, T., Hansen, N., Qi, F., Westbrook, C.K., and Westmoreland, P.R., *Angew. Chem.*, 2010, vol. 49, p. 3572.
15. Lemaire, R., Therssen, E., and Desgroux, P., *Fuel*, 2010, vol. 89, p. 3952.
16. Parag, S. and Raghavan, V., *Combust. Flame*, 2009, vol. 156, p. 997.
17. Frassoldati, A., Faravelli, T., Ranzi, E., and Kohse-Hoinghaus, K., *Combust. Flame*, 2011, vol. 158, p. 1264.
18. Therrien, R.J., Ergut, A., Levendis, Y.A., Richter, H., Howard, J.B., and Carlson, J.B., *Combust. Flame*, 2010, vol. 157, p. 296.
19. Korobeinichev, O.P., Yakimov, S.A., Knyazkov, D.A., Bolshova, T.A., Shmakov, A.G., Yang, J., and Qi, F., *Proc. Combust. Inst.*, 2011, vol. 33, p. 569.
20. Heufer, K.A., Bugler, J., and Curran, H.J., *Proc. Combust. Inst.*, 2013, vol. 34, p. 511.
21. Couli, S., Lois, E., and Stournas, S., *Energy Fuels*, 1998, vol. 12, p. 918.
22. Rakopoulos, C.D., Antonopoulos, K.A., Rakopoulos, D.C., Hountalas, D.T., and Andritsakis, E.C., *Int. J. Altern. Propul.*, 2007, vol. 1, p. 309.
23. Tang, C., Wei, L., Man, X., Zhang, J., Huang, Z., and Law, C.K., *Combust. Flame*, 2013, vol. 160, p. 520.
24. Yeung, C. and Thomson, M.J., *Proc. Combust. Inst.*, 2012, vol. 34, p. 795.
25. Cann, A.F. and Liao, J.C., *Appl. Microbiol. Biotechnol.*, 2010, vol. 85, p. 893.
26. Tsujimura, T., Pitz, W.J., Yang, Y., and Dec, J.E., *SAE*, 2011, 2011-24-0023.
27. Zhang, J., Niu, S., Zhang, Y., Tang, C., Jiang, X., Hu, E., and Huang, Z., *Combust. Flame*, 2013, vol. 160, p. 31.
28. McEnally, C.S. and Pfefferle, L.D., *Proc. Combust. Inst.*, 2005, vol. 30, p. 1363.
29. Yang, B., Osswald, P., Li, Y., Wang, J., Wei, L., Tian, Z., Qi, F., and Kohse-Hoeinghaus, K., *Combust. Flame*, 2007, vol. 148, p. 198.
30. Sarathy, S.M., Thomson, M.J., Togbe, C., Dagaut, P., Halter, F., and Mounaim-Rousselle, C., *Combust. Flame*, 2009, vol. 156, p. 852.
31. Grana, R., Frassoldati, A., and Faravelli, T., *Combust. Flame*, 2010, vol. 157, p. 2137.
32. Osswald, P., Gueldenberg, H., Kohse-Hoeinghaus, K., Yang, B., Yuan, T., and Qi, F., *Combust. Flame*, 2011, vol. 158, p. 2.
33. Agathou, M. and Kyritsis, D.C., *Fuel*, 2011, vol. 90, p. 255.

34. Hansen, N., Harper, M.R., and Green, W.H., *Phys. Chem. Chem. Phys.*, 2011, vol. 13, p. 20262.
35. Harper, M.R., Van Geem, K.M., Pyl, S.P., Marin, G.B., and Green, W.H., *Combust. Flame*, 2011, vol. 158, p. 16.
36. Veloo, P.S. and Egolfopoulos, F.N., *Proc. Combust. Inst.*, 2011, vol. 33, p. 987.
37. Camacho, J., Lieb, S., and Wang, H., *Proc. Combust. Inst.*, 2013, vol. 34, p. 1853.
38. Moss, J.T., Berkowitz, A.M., Oehlschlaeger, M.A., Biet, J., Warth, V.R., Glaude, P.A., and Battin-Leclerc, F., *J. Phys. Chem. A*, 2008, vol. 112, p. 10843.
39. Dagaut, P. and Togbe, C., *Fuel*, 2008, vol. 87, p. 3313.
40. Dagaut, P. and Togbe, C., *Energy Fuels*, 2009, vol. 23, p. 3527.
41. Dagaut, P., Sarathy, S.M., and Thomson, M.J., *Proc. Combust. Inst.*, 2009, vol. 32, p. 229.
42. Togbe, C., Mze-Ahmed, A., and Dagaut, P., *Energy Fuels*, 2010, vol. 24, p. 5244.
43. Norton, T.S. and Dryer, F.L., *Symp. Int. Combust.*, 1991, vol. 23, p. 179.
44. Lefkowitz, J.K., Heyne, J.S., Won, S.H., Dooley, S., Kim, H.H., Haas, F.M., Jahangirian, S., Dryer, F.L., and Ju, Y., *Combust. Flame*, 2012, vol. 159, p. 968.
45. Welz, O., Savee, J.D., Eskola, A.J., Sheps, L., Osborn, D.L., and Taatjes, C.A., *Proc. Combust. Inst.*, 2013, vol. 34, p. 493.
46. Johnson, M.V., Goldsborough, S.S., Serinyel, Z., O'Toole, P., Larkin, E., O'Malley, G., and Curran, H.J., *Energy Fuels*, 2009, vol. 23, p. 5886.
47. Noorani, K.E., Akih-Kumgeh, B., and Bergthorson, J.M., *Energy Fuels*, 2010, vol. 24, p. 5834.
48. Black, G., Curran, H.J., Pichon, S., Simmie, J.M., and Zhukov, V., *Combust. Flame*, 2010, vol. 157, p. 363.
49. Heufer, K.A., Fernandes, R.X., Olivier, H., Beeckmann, J., Roehl, O., and Peters, N., *Proc. Combust. Inst.*, 2011, vol. 33, p. 359.
50. Liu, W., Kelley, A.P., and Law, C.K., *Proc. Combust. Inst*, 2011, vol. 33, p. 995.
51. Karwat, D.M.A., Wagnon, S.W., Teini, P.D., and Wooldridge, M.S., *J. Phys. Chem. A*, 2011, vol. 115, p. 4909.
52. Stranic, I., Chase, D.P., Harmon, J.T., Yang, S., Davidson, D.F., and Hanson, R.K., *Combust. Flame*, 2011, vol. 159, p. 516.
53. Vranckx, S., Heufer, K.A., Lee, C., Olivier, H., Schill, L., Kopp, W.A., Leonhard, K., Taatjes, C.A., and Fernandes, R.X., *Combust. Flame*, 2011, vol. 158, p. 1444.
54. Veloo, P.S., Wang, Y.L., Egolfopoulos, F.N., and Westbrook, C.K., *Combust. Flame*, 2010, vol. 157, p. 1989.
55. Frassoldati, A., Grana, R., Faravelli, T., Ranzi, E., Osswald, P., and Kohse-Hoinghaus, K., *Combust. Flame*, 2012, vol. 159, p. 2295.
56. Sarathy, S.M., Vranckx, S., Yasunaga, K., Mehl, M., Osswald, P., Metcalfe, W.K., Westbrook, C.K., Pitz, W.J., Kohse-Hoinghaus, K., Fernandes, R.X., and Curran, H.J., *Combust. Flame*, 2012, vol. 159, p. 2028.
57. Hsieh, W.D., Chen, R.H., Wu, T.L., and Lin, T.H., *Atmos. Environ.*, 2002, vol. 36, p. 403.
58. Yuksel, F. and Yuksel, B., *Renew. Energy*, 2004, vol. 29, p. 1181.
59. Gravalos, I., Moshou, D., Gialamas, Th., Xyradakis, P., Kateris, D., and Tsiropoulos, Z., *Renew. Energy*, 2013, vol. 50, p. 27.
60. Costagliola, M.A., Simio, L.D., Iannaccone, S., and Prati, M.V., *Appl. Energy*, 2013, vol. 111, p. 1162.
61. Aleiferis, P.G., Serras-Pereira, J., and Richardson, D., *Fuel*, 2013, vol. 109, p. 256.
62. He, B.Q., Shuai, S.J., Wang, J.X., and He, H., *Atmos. Environ.*, 2003, vol. 37, p. 4965.
63. Can, O., Celikten, I., and Usta, N., *Energy Convers. Manage.*, 2004, vol. 45, p. 2429.
64. Rakopoulos, D.C., Rakopoulos, C.D., Giakoumis, E.G., Dimaratos, A.M., and Kyritsis, D.C., *Energy Convers. Manage.*, 2010, vol. 51, p. 1989.
65. Rakopoulos, D.C., Rakopoulos, C.D., Papagiannakis, R.G., and Kyritsis, D.C., *Fuel*, 2011, vol. 90, p. 1855.
66. Lujaji, F., Kristof, L., Bereczky, A., and Mbarawa, M., *Fuel*, 2011, vol. 90, p. 505.
67. Valentino, G., Corcione, F.E., Iannuzzi, S.E., and Serra, S., *Fuel*, 2012, vol. 92, p. 295.
68. Sukjit, E., Herreros, J.M., Dearn, K.D., Tsolakis, A., and Theinnoi, K., *Int. J. Hydrogen Energy*, 2013, vol. 38, p. 1624.
69. Yoshimoto, Y., Kinoshita, E., Shanbu, L., and Ohmura, T., *Energy*, 2013, vol. 61, p. 44.
70. Jin, H., Wang, Y., Zhang, K., Guo, H., and Qi, F., *Proc. Combust. Inst.*, 2013, vol. 34, p. 779.
71. Melius, C.F., Colvin, M.E., Marinov, N.M., Pitz, W.J., and Senkan, S.M., *Symp. Int. Combust.*, 1996, vol. 26, p. 685.
72. Hwang, J.Y., Lee, W., Kang, H.G., and Chung, S.H., *Combust. Flame*, 1998, vol. 114, p. 370.
73. Yang, B., Huang, C., Wei, L., Wang, J., Sheng, L., Zhang, Y., Qi, F., Zheng, W., and Li, W.K., *Chem. Phys. Lett.*, 2006, vol. 423, p. 321.
74. Liu, F., Xu, Y., Liu, J., Liu, D., Li, J., Zhang, G., Li, X., Zou, S., and Lai, S., *Atmos. Environ.*, 2013, vol. 69, p. 265.
75. Čupr, P., Flegrová, Z., Franců, J., Landlová, L., and Klánová, J., *Environ. Int.*, 2013, vol. 54, p. 26.
76. Velásquez, M., Mondragón, F., and Santamaría, A., *Fuel*, 2013, vol. 104, p. 681.
77. Detilleux, V. and Vandooren, J., *Combust. Sci. Technol.*, 2008, vol. 180, p. 1347.
78. Szeliga, J. and Dipple, A., *Chem. Res. Toxicol.*, 1998, vol. 11, p. 1.
79. Vereecken, L. and Peeters, J., *Phys. Chem. Chem. Phys.*, 2003, vol. 5, p. 2807.
80. Brukh, R., Salem, T., Slanvetpan, T., Barat, R., and Mitra, S., *Adv. Environ. Res.*, 2002, vol. 6, p. 359.
81. Frenklach, M. and Warnatz, J., *Combust. Sci. Technol.*, 1987, vol. 51, p. 265.
82. Wang, D., Violi, A., Kim, D.H., and Mullholland, J.A., *J. Phys. Chem. A*, 2006, vol. 110, p. 4719.
83. Lu, M. and Mullholland, J.A., *Chemosphere*, 2001, vol. 42, p. 625.

84. Violi, A., Sarofim, A.F., and Truong, T.N., *Combust. Flame*, 2001, vol. 126, p. 1506.

85. Violi, A., Sarofim, A.F., and Truong, T.N., *Combust. Sci. Technol.*, 2002, vol. 174, p. 205.

86. D'Anna, A. and Kent, J.H., *Combust. Flame*, 2003, vol. 132, p. 715.

87. Hansen, N., Klippenstein, S.J., Taatjes, C.A., Miller, J.A., Wang, J., Cool, T.A., Yang, B., Yang, R., Wie, L., Huang, C., Wang, J., Qi, F., Law, M.E., and Westmoreland, P.R., *J. Phys. Chem. A*, 2006, vol. 110, p. 3670.

88. Kee, R.J., Grcar, J.F., Smooke, M.D., and Miller, J.A., *ReportSAND85-8240*, Albuquerque, N.M.: Sandia National Laboratories, 1985.

89. Richter, H. and Howard, J.B., *Phys. Chem. Chem. Phys.*, 2002, vol. 4, p. 2038.

90. Bhargava, A. and Westmoreland, P.R., *Combust. Flame*, 1998, vol. 115, p. 456.

91. Bhargava, A. and Westmoreland, P.R., *Combust. Flame*, 1998, vol. 113, p. 333.

92. Westmoreland, P.R., *PhD Thesis*, Cambridge: *Massachusetts Inst. of Technology*, 1986.

93. Benish, T.G., *PhD Thesis*, Cambridge: *Massachusetts Inst. of Technology*, 1999.

94. Bittner, J.D. and Howard, J.B., *Proc. Combust. Inst.*, 1981, vol. 18, p. 1105.

95. Weber, B., Kumar, K., Zhang, Y., and Sung, C., *Combust. Flame*, 2011, vol. 158, p. 809.

96. Defoeux, F., Dias, V., Renard, C., Van Tiggelen, P.J., and Vandooren, J., *Proc. Combust. Inst.*, 2005, vol. 30, p. 1407.

97. Detilleux, V. and Vandooren, J., *Combust. Explos. Shock Waves*, 2009, vol. 45, p. 392.